Towards Patient-specific SAR Calculation for Parallel Transmission Systems

I. Graesslin[1], S. Wang[2], S. Biederer[3], G. Mens[4], B. Annighoefer[5], H. Homann[1], J. Duyn[2], and P. Harvey[4]
[1]Philips Research Europe, Hamburg, Germany, [2]NINDS, National Institutes of Health, Bethesda, MD, United States, [3]Institute of Medical Engineering, University of Lübeck, Lübeck, Germany, [4]Philips Healthcare, Best, Netherlands, [5]TU Hamburg-Harburg, Hamburg, Germany

Introduction The safety assessment via the specific absorption rate (SAR) is a prerequisite for in vivo MRI experiments. In parallel transmission, such an assessment is non-trivial, since the local SAR distribution does not only depend on the individual patient anatomy, but also on the multi-channel excitation. In general, patient safety can be achieved by carrying out simulation-based SAR calculations before the scan and by monitoring the deviation from the desired waveform during the scan. In case of violations of the SAR limits [1] or any unsafe conditions, the scan is aborted [2]. Typically, such SAR calculations rely on generic patient models and on the evaluation of worst-case scenarios requiring a broad safety margin. The use of patient-specific SAR calculations allows a more efficient exploitation of the respective limits and can improve imaging performance. The required calculation essentially consists of three parts: 1) Patient-specific model generation, 2) fast calculation of the electric fields for each transmit coil of the RF array [3], and 3) a real-time computation of the actual pulse-dependent local SAR distribution [4]. This paper presents the general concept of patient-specific SAR calculations and describes the implementation of the real-time SAR computation.

Methods An overview of the general concept is given by the flowchart in Fig. 1. The process starts with a patient-specific body model, which can be obtained either from a corresponding database or from data measured during a pre-scan. The necessary dielectric body models can be obtained from MR images, for instance via an intensity-based transfer function [5] or via body-fat separated images [6].

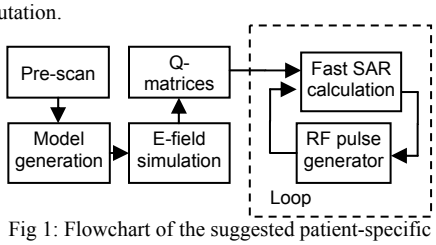

Fig 1: Flowchart of the suggested patient-specific SAR calculation concept

In the next step, the E-fields inside the body are calculated. Conventionally, finite-difference time-domain (FDTD) techniques are used for this purpose. These methods, however, are rather slow for calculations on real patient data. Instead, a new and fast method based on the surface integral-equation (SIE) method [7] is proposed. The method consists of three steps: 1) applying a fast integral-equation method to obtain magnetic field distributions with a homogeneous phantom filled with a single equivalent medium 2) calculating magnetic fields at a set of Cartesian grid points inside phantom 3) replacing the single medium with inhomogeneous tissue and applying Ampere's law Eq. (1) for the calculation of the electric field distributions. The last step is accomplished via a standard finite-difference scheme. This method allows a fast calculation of the patient-specific SAR.

$$E_m = \nabla \times H_m / (\sigma + i\omega\varepsilon) \quad (1)$$

$$Q_{mn} = \sum_{10g} E_m^H \cdot E_n \quad (2)$$

$$SAR_{10g} = \sum_{m,n} I_m^H \cdot Q_{mn} \cdot I_n \quad (3)$$

For efficient SAR calculation, the quadratic terms of the E-fields for all TX-element combinations (m,n) are pre-calculated, averaged over the local test volume (typ. 10g of tissue) and stored in the so-called Q-matrices (Eq. 2). Given any exam-dependent multi-channel RF pulse I (e.g. B1-mapping, RF shimming, spatially selective pulses, etc.), the local SAR is then calculated for every parameter change in the scanner user-interface or iteration of the pulse-optimization step (Eq. 3).

The calculation of the E-fields was performed a) using the Fast Integral Equation Method for an 8-channel 7T head TX coil using an inhomogeneous human head model (Virtual Family Mode, ITIS Foundation, Switzerland) which took several minutes and b) using finite-difference time-domain simulations ("XFDTD", Remcom Inc., USA) for an ideally decoupled 3T multi-channel body coil (MBC) [8]. Different head and body models (resolution: 5mm) were used for the field calculations, including rescaled versions of the "Visible Human Male" [9] as well as models segmented from MR imaging data.

The real-time SAR calculation part of the concept was implemented on an 8-channel transmit 3T MRI system ([10], Achieva, Philips Healthcare, The Netherlands). The Q-matrices were used for a calculation of the global and local SAR. To achieve the SAR calculation in real-time, it is implemented with the Compute Unified Device Architecture (CUDA) on a high performance graphics card (GTX295, NVIDIA® Corporation, USA) with 2×240 processors. The card was integrated into the acquisition and processing unit of the system. A number of in vivo experiments were carried out, including basic RF shimming (450×270×75 mm³ FOV, 64×38×5 matrix, angle = 60°, TR1 = 20 ms, TR2 = 100 ms, TE = 2.3 ms) as well as spatially selective RF pulses (spiral k-space trajectories, numerical field-of-excitation of 32×32 pixels, reduction factors R up to 7). The SAR reduction of the RF pulses was carried out using the optimization described in [11] as well as in [12] extended with temporal averaging according to [11].

Results and Discussion RF Pulse optimization using a patient specific SAR model enables to include patient adaptive SAR management. This process can take place in an iterative manner, where the estimated SAR is fed back into the RF pulse optimization as shown in fig. 1. The results of the fast field simulations by SIE and Ampere's law are shown in Fig. 2. The B1 field distribution calculated by the integral-equation method is shown in the middle, while the electric field distribution calculated via Ampere's law is shown on the right side. The two white blocks in the left figure denote coil conductor locations. An example of a SAR hotspot suppression resulting in a reduction of 56% is illustrated in Fig. 3. RF Shimming experiments were carried out as shown in Fig. 4. On the left side an image of the target anatomy for the B1 maps is shown. In the middle the result of a quadrature shim settings is illustrated, while on the right side an adapted shim settings derived from the measured B1 can be seen. An improvement in homogeneity of 60% compared to the quadrature excitation was achieved.

Thus, a proof of principle of a patient-specific SAR calculations concept was given. In a next step, a further comparison with conventional local SAR estimation techniques is required as well as its validation, which is however, non-trivial.

Conclusion A field-strength independent concept for patient-specific SAR calculation was presented, and examples of SAR distributions were shown for 3T and 7T using the XFDTD and a new version of a fast Surface Integral Equation Method, respectively. After the fast generation of the SAR-matrices from the E-fields, accurate SAR determination is carried out in real-time to conform to existing safety standards ensuring SAR-related patient safety for parallel RF transmission. The real-time part of the concept was implemented on an 8-channel TX MRI scanner, and in vivo RF shimming experiments were demonstrated. Furthermore, the concept was applied to spatially selective pulses. The proposed concept makes patient-specific SAR calculations feasible in the near future.

Acknowledgements We would like to thank Z. Zhai and M. Morich, Philips Healthcare, Cleveland, USA as well as D. Brunner and K. Pruessmann, University and ETH Zurich, Zurich, Switzerland for discussions and support.

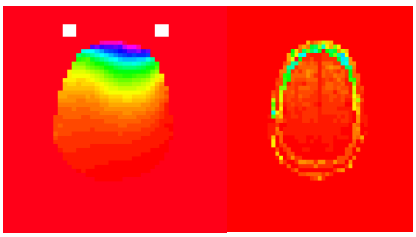
Fig. 2: Calculated magnetic (left) and electric (right) fields, using fast field simulation by SIE and Ampere's law.

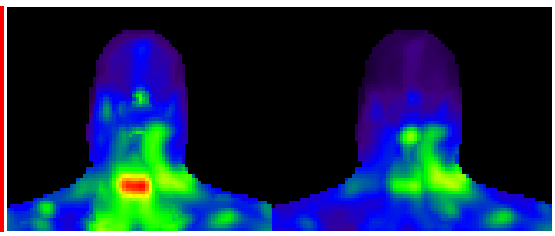
Fig. 3: 2D MIP of spatial SAR distribution for spatially selective pulses (before and after SAR optimization).

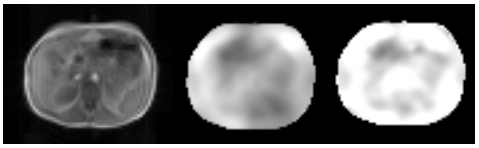
Fig. 4: RF Shimming for an 8-channel TX system: the image shows the target anatomy for the B1 maps (left), quadrature shim settings (middle) and adapted shim settings derived from the measured B1 (right).

References

[1] IEC [2002] 60601-2-33, 2nd Ed.
[2] Graesslin I, et al. [2008] ISMRM 16:74
[3] Shumin W, et al. [2006] PMB 51:3211-3229
[4] Graesslin I, et al. [2007] ISMRM 15:1086
[5] Mazzurana M, et al. [2003] PMB 48:3157–3170
[6] Homann H, et al. [2009] ESMRMB 195
[7] Wang S, et al. [2009] ISMRM 17:506
[8] Vernickel P, et al. [2007] MRM 58(2):381-9
[9] NLM [1996] "Visible Human Project"
[10] Graesslin I, et al. [2006] ISMRM 14:129
[11] Graesslin I, et al. [2009] ISMRM 17:176
[12] Brunner D, et al. [2009] ISMRM 17:176